Day-Ahead and Intraday Forecasts of the Dynamic Line Rating for Buried Cables

IEEE Access
Multidisciplinary | Rapid Review | Open Access Journal

Received November 12, 2018, accepted December 7, 2018, date of publication December 18, 2018,
date of current version January 11, 2019.

*Digital Object Identifier 10.1109/ACCESS.2018.2888505*

# Day-Ahead and Intraday Forecasts of the Dynamic Line Rating for Buried Cables

**ANTONIO BRACALE[1], (Senior Member, IEEE), PIERLUIGI CARAMIA[1], PASQUALE DE FALCO[1], (Member, IEEE), ANDREA MICHIORRI[2], AND ANGELA RUSSO[3], (Senior Member, IEEE)**

[1]Department of Engineering, University of Napoli Parthenope, 80143 Naples, Italy
[2]Centre procédés, énergies renouvelables et systèmes énergétiques, Mines ParisTech, PSL University, 06904 Paris, France
[3]Department of Energy, Politecnico of Torino, 10129 Turin, Italy

Corresponding author: Pasquale De Falco (pasquale.defalco@uniparthenope.it)

This work was supported by the University of Napoli Parthenope in the framework of Bando per il sostegno alla ricerca individuale per il triennio 2015–2017 and Bando di ricerca competitiva per il triennio 2016–2018.

**ABSTRACT** Forecasting the dynamic line rating allows to reach peaks of operational excellence upon electrical networks. Literature on dynamic rating has mainly addressed overhead lines, whereas lesser attention has been paid to buried cables. However, modeling the dynamics of the cable-soil system is quite a challenge, especially when both the day-ahead and intraday forecasting scenarios have to be considered in order to suit the usual operating tasks on electrical grids. This paper aims at providing a comparison among different forecasting methods, specially developed for such lead times. In particular, this paper: 1) develops a new physical-statistical method for intra-day forecasting scenarios; and 2) verifies the suitability of a data-driven method, which is an adaption of the state-of-the-art approach for dynamic overhead-line rating to the case of dynamic buried-cable rating, for both intraday and day-ahead scenarios. Numerical applications based on actual data are presented to validate the comparative study, and the forecasting results are compared with a naïve benchmark based on the persistence method.

**INDEX TERMS** Forecasting, power distribution lines, regression analysis.

## I. INTRODUCTION

Distribution systems are incurring a rapid and substantial transformation. The overall energy demand is steadily increasing, and the distributed generators (DGs) installed at medium and low voltage levels of the networks inject powers that can bi-directionally flow through lines and equipment. The structure of existing distribution networks typically is not designed for such a configuration, thus limiting the potential development and installation of DGs and driving the energy management toward non-optimal solutions.

Upgrading the distribution networks is the customary solution to lighten these burdens; it brutally consists in replacing or installing additional lines, with a huge investment of capitals and with invasive actions upon grids. Moreover, it also involves spatial and environmental issues that often block the entire project, but, more importantly, it is not always the most practical solution. Indeed, conductors are often underused, since they do not work at rated design temperatures, nor at rated environmental conditions [1], [2]. The ability to increase the usage of existing conductors is denoted Dynamic Line Rating (DLR), and it consists in pushing the current that can flow through a conductor up to a maximum allowable value, without pushing the thermal stress beyond the rated one [3]. This obviously is not exempt from technical complexities, although it requires smaller economical investments (e.g., the installation of sensors and smart circuit breakers) than upgrading distribution networks.

DLR is usually developed for cables by fixing a target operating temperature[1] for the conductor, dynamically adapting the current to the time-varying environmental and load conditions. This deviates from the traditional concept of static line rating which assumes static thermal and environmental conditions throughout the whole life of the conductor; it is a simplifying assumption in the design step, that however leads to underusing the lines when operating them. Indeed, favorable environmental conditions (e.g., smaller ambient

[1]It is a common practice to select the target operating temperature as the temperature corresponding to the rated life of the cable (e.g., 20 years) through the Arrhenius equation. When the target operating temperature is not specifically provided by the cable manufacturer, relevant standards [4] list the reference values for different types of insulation (e.g., 70°C for PVC insulated cables, and 90°C for EPR/XLPE insulated cables).

temperatures) or favorable load conditions (e.g., small currents flowing through the conductor for long periods) allow to increase the maximum loadability of the conductor beyond its static line rating in a fixed time interval, without exceeding the conductor target operating temperature.

Overhead Line (OHL) DLR is a state-of-the-art concept, and mature theoretical and practical applications have been developed by researchers and practitioners to transmission networks [3], [5], [6]. DLR for Underground Cables (UGC) is instead a to-be-developed concept, that has recently started attracting the interest of practitioners [7]–[9] and distribution system operators [10], [11]. UGC DLR retains many of the technical challenges of OHL DLR, but it is furthermore complicated by the need of estimating the time-varying conditions of the surrounding soil. These may depend on several environmental phenomena (precipitations, ambient temperature, degree of saturation) that have to be properly addressed before taking any actions on these systems.

The target time horizons of the DLR follow the target time horizons of the energy dispatching in distribution systems, which is usually scheduled at intraday (1- to 12-hour lead time) and day-ahead (13- to 36-hour lead time) time scales. The environmental phenomena may have a smaller or a greater impact upon the UGC DLR at different time horizon; for example, the diffusion of water through the soil caused by rain is not instantaneous and it is driven by slow dynamics, thus it requires hours to give effects upon the UGC DLR. Thus, separate approaches for intraday and day-ahead UGC DLR are required in order to capture different dynamics.

This paper has two main objectives. The first consists of a new proposal for the intraday UGC DLR forecasting, relying on an accurate modeling of the cable-soil thermal-hydraulic dynamics and on machine learning forecasts of the input variables. The second consists in testing the effectiveness of a data-driven UGC DLR forecasting method, starting from a state-of-the-art approach originally suited for OHL DLR, applied both to the intraday and the day-ahead scenarios.

This paper is organized as it follows. A review of the existing contributions on intraday and day-ahead UGC DLR is presented in Section II, together with the description of the main innovations of this paper. The methods proposed and tested for UGC DLR are described in Section III, together with a description of the thermal-hydraulic model of the soil, and with the description of the forecasting systems used for intraday and day-ahead scenarios. The data used for the numerical applications are commented in Section IV, whereas the results of the proposed methods are presented and discussed in Section V. Eventually, our conclusions are reported in Section VI.

## II. STATE OF THE ART AND CONTRIBUTIONS TO KNOWLEDGE

Researchers and system operators have chiefly addressed OHL DLR in their studies. Contributions on UGC DLR are more recent, but they have started drawing the interest of the scientific community due to the increasing requests in the versatility of distribution systems, to account for the increased demand and for the widespread presence of DGs, mainly in the context of the Smart Grid paradigm. In this Sections, the main contributions on intraday and day-ahead UGC DLR are discussed, in order to clarify the innovations brought by our proposed method.

### A. STATE OF THE ART ON UGC DLR INTRADAY AND DAY-AHEAD FORECAST

Degefa *et al.* [1] developed a method for forecasting the dynamic thermal state of several distribution network components (OHLs, UGCs, and distribution transformers), for lead times ranging from 1 to 24 hours before (thus covering the intraday and, partially, the day-ahead). The methodology consisted in forecasting some of the environmental variables that were considered to be relevant for the dynamic thermal state; in the case of UGCs, the only considered variable was the soil temperature, forecasted through an ARIMA model. A seven-loop model was used to estimate the cable-soil thermal exchange, in order to produce the cable temperature forecasts. However, the paper did not provide DLR forecasts, but only forecasts of cable thermal states.

The method proposed in [12] and [13] did not consider any variation of the soil thermal resistivity, nor of the soil temperature; it instead updated the forecasts of UGC DLR at each hour, adjusting it by means of cable load SVR-based forecasts. Huang *et al.* [12] forecast a 6-hour emergency rating obtained through the IEC cable-soil thermal model, whereas in [13] they forecast 1-hour, 6-hour and 24-hour emergency ratings obtained through finite-element, IEC, and Cigrè thermal models.

An inverse approach based on distributed temperature sensing was presented in [14] and [15]. Here the authors exploited temperature measurements in order to estimate soil parameters (i.e., thermal resistivity and temperature) in an optimization framework; then, the UGC DLR was obtained from these estimated parameters by means of a finite-element cable-soil thermal model.

Reference [16] investigated the effect of weather conditions on the UGC DLR. In particular, precipitation and soil temperature were estimated by means of physical models, and the resulting DLR was obtained through the steady-state solution of the IEC cable-soil thermal transient. A similar investigation to address the effect of the variation of the soil moisture on the UGC DLR was presented in [17] and [18], although using cable temperature measurements. These papers adopted a thermal model based on thermoelectric equivalents, dividing insulation, jacket, and surrounding soil in different zones (in a procedure similar to the finite-element method).

### B. CONTRIBUTIONS TO KNOWLEDGE

The analysis of the works described above helps to define several research questions that this paper aims at answering.

A first limitation of the works listed above consists in their focus on a single forecast model, and often a single test case is considered. In this paper, several models are compared and

evaluated along the same metrics, in order to understand the benefits and drawbacks of each of them. Furthermore, thanks to the availability of a soil dynamic model, UGC DLRs are simulated for two scenarios: a cable buried in clay and a cable buried in sand.

A second limitation is represented by the lack of information on longer forecast horizons, which makes difficult to apply the presented forecast models in day-ahead scenarios. In fact, considering that eventual operation planning must be made in the afternoon of the day before, UGC DLR forecasts must be available roughly by noon, imposing forecasts horizons from 1 to 36 hours.

Eventually, the literature lacks any assessment on the accuracy of existing OHL DLR forecasting methods, based on Numerical Weather Predictions (NWP), when they are specifically adapted to the UGC DLR framework. In fact, although the weather is commonly associated with atmospheric phenomena in OHL DLR, it involves also the upper layer of the soil, and information about soil temperature and soil water content, available at different depths, are useful for the UGC DLR. Since literature on OHL DLR is much more mature than the literature on UGC DLR, investigating the applicability of existing OHL solutions (adequately adapted to the UGC case) could be fruitful.

This paper, therefore:

- explores the behavior and performance of different forecast methods, clarifying their advantages and disadvantages;
- proposes and tests a new physical-statistical forecast method, which is specifically developed for lead times up to 12 hours (intra-day forecast);
- proposes and tests the effectiveness of a data-driven forecast method, developed from a state-of-the-art OHL DLR forecasting approach [19], [20], for 1- to 12-hours (intraday) and for 13- to 36-hours (day-ahead) lead times; this allows also to explore the contribution of NWPs of soil thermal and hydraulic parameters in UGC DLR forecasting.

## III. MODELING

Two methods are presented in this section:

- a physical-statistical method (PSM), specifically developed for forecasting the UGC DLR at intraday scenarios;
- a data-driven method (DDM), adapted for intraday and day-ahead scenarios.

The forecasts of 1-hour rating are considered in the following, although the procedures could be easily extended to longer interval ratings.

Common inputs to both methods are precipitation historical data, soil temperature historical data at an upper layer,[2] cable load historical data, the soil parameters, cable parameters (among them, the cable target operating temperature), and calendar variables. Further inputs, if available, could be used as exogenous predictors, in order to improve the results of the forecasting systems; in particular, the effectiveness of NWPs is investigated for the DDM case. We will discuss these in details in the corresponding sub-Sections.

In the following, we will denote with $h$ the forecast time horizon (in hours), with $h - k$ the forecast start time, and consequently with $k$ the forecast lead time. Each hour is further discretized in $F$ equally-spaced time intervals, in order to capture the dynamics of fast variables and parameters (i.e., the variables that cannot be reasonably assumed to be constant during an hour). Therefore, the whole forecast lead time is made of $kF$ intervals ($t = t_1, t_2, \ldots, t_{kF}$).

The proposed methods are based on different approaches.

The PSM proposed for intraday forecast scenarios ($1 \leq k \leq 12$) consists in:

- building Support Vector Regression (SVR) based forecasts of soil temperature at the upper layer, precipitation, and cable load throughout the whole forecast lead time (i.e., k individual forecasts for each variable);
- using SVR forecasts of the environmental conditions in a thermal-hydraulic model of the soil, in order to obtain estimations throughout the whole forecast lead time of the soil dynamic characteristics (i.e., soil temperature at the burial depth, soil thermal resistivity, and soil thermal diffusivity) that influence the cable-soil thermal exchange;
- forecasting the UGC DLR at the target hour h, applying the IEC cable-soil thermal model, fixing the maximum temperature of the cable at the target operating temperature during the hour h.

The DDM tested for intraday ($1 \leq k \leq 12$) and day-ahead ($12 < k \leq 36$) forecast scenarios consists in:

- using the historical measurement and historical weather forecasts of precipitation and soil temperature at the upper layer, in order to get estimated data of soil temperature at the burial depth, soil thermal resistivity, and soil thermal diffusivity by means of the thermal-hydraulic model of the soil during the entire available history;
- estimating historical UGC DLR data through the IEC cable-soil thermal model in transient conditions;
- forecasting the UGC DLR at the target hour h, using a regression model on historical UGC DLR data.

Figure 1 shows the diagram flows of the proposed methods. It is important to note that both the proposed UGC DLR forecasting methods allow to predict the DLR at a specific section of the route of the cable circuit. When dealing with a very long route, or in general with sensibly varying conditions along the route, the suggested solution is to investigate the locations along the cable route characterized by the most critical thermal conditions (i.e., "hottest-spots" along the route), as in [14] and [17].

[2] Soil temperature could be measured at ground level or at a generic depth (up to the cable burial depth). In order to generalize the procedure also in the cases in which soil temperature is measured at a generic depth, we will refer to "upper layer" as the soil layer at which soil temperature is measured, denoting the height of the soil column with $z = z_1$.

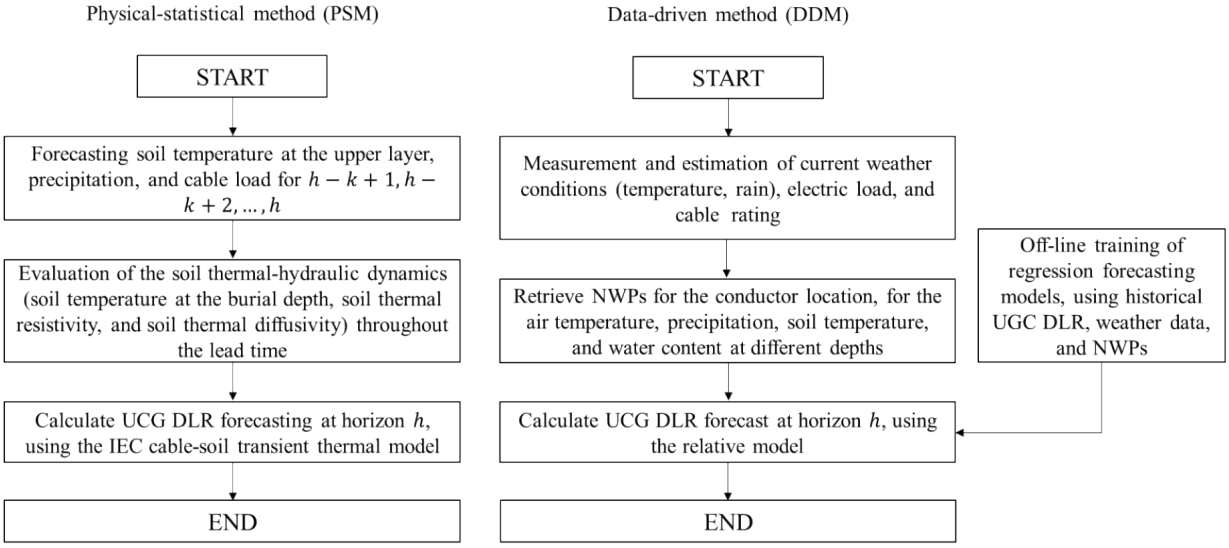


**FIGURE 1.** Diagram flow of the proposed UGC DLR forecasting methods.

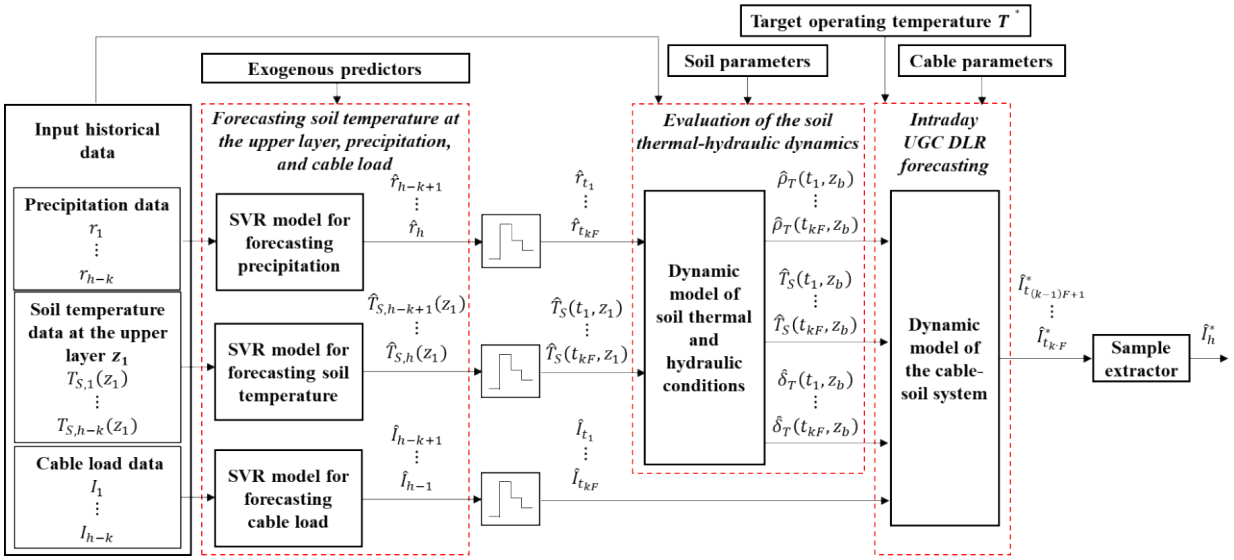


**FIGURE 2.** Block scheme of the physical-statistical method proposed for intraday UGC DLR forecasting.

### A. PHYSICAL-STATISTICAL METHOD FOR INTRADAY UGC DLR FORECASTING

The detailed steps of the PSM for UGC DLR intraday forecasting are illustrated in Figure 2.

The input historical data is made of observations of precipitation, soil temperature measured at the upper layer, and cable load collected until the forecast start time $h-k$. Other relevant exogenous predictors (e.g., weather variables, weather forecasts, calendar variables) are used in order to forecast precipitation, soil temperature at the upper layer, and cable load throughout the whole forecast lead time, by means of SVR models. To avoid unnecessary complications, only one forecast of each of these three variables is produced for each hour of the lead time, and that forecast is put on hold during the sub-hourly time discretization. This allows to reduce the overall computational burden of the proposed method (only $3k$ forecasts are needed, whereas $3kF$ forecasts would be necessary in a complete approach).

Forecasts of precipitation and soil temperature at the upper layer are used in the thermal-hydraulic model of the soil, in order to capture the dynamics of the soil thermal resistivity, soil thermal diffusivity, and soil temperature at the burial depth, throughout the whole lead time. Note that these variables are returned for $t = t_1, \ldots, t_{kF}$.

Eventually, forecasts of the cable load and estimations of soil thermal conditions are used in the dynamic model of the

cable-soil system, in order to give forecasts of the UGC DLR, assigning the target operating temperature of the cable.

The three main steps of the scheme in Fig. 2 are backwards discussed in the following sub-Sections, in order to better clarify the proposed approach. It is worth to note that the proposed intra-day method is computationally intensive; its applicability for longer time horizons (up to the 36 hours of the day-ahead scenario) needs further development. In our experiments, we managed to get results only up to 16 hours ahead, before the computational time exceeded the forecast lead time, thus making the procedure inapplicable in real-world scenarios for longer lead times.

### 1) DYNAMIC MODEL OF THE CABLE-SOIL SYSTEM

The IEC cable-soil thermal model is briefly discussed in this sub-Section. In order to streamline the problem, we overlook insulation, sheath and armour losses in the cable[3]; under these conditions, the multi-loop electrical network representative of the short-duration thermal transient is the one illustrated in Figure 3.

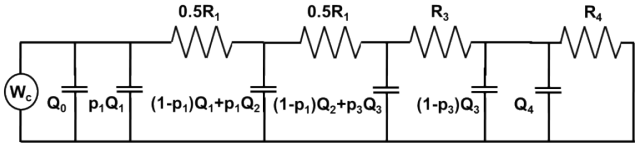


**FIGURE 3. Equivalent multi-loop electrical network of the cable-soil system in short-duration thermal transient.**

$W_c$ represents the electrical resistive losses in the conductor, $Q_0$ is the thermal capacitance of the metallic conductor, $Q_1$ and $Q_2$ are representative of the thermal capacitance the insulation (the insulation thermal capacitance is split in two terms, according to [22]), $Q_3$ is the thermal capacitance of the jacket, $Q_4$ is the thermal capacitance surrounding soil, $R_1$ is the thermal resistance of the insulation, $R_3$ is the thermal resistance of the jacket, $R_4$ is the thermal resistance of the surrounding soil, and $p_1, p_2$ are van Wormer coefficients for insulation and jacket, respectively.

For a cable with $n_c$ active cores, the electrical losses are calculated as:

$$W_c(t) = n_c R_{el_{20}} \{1 + \alpha_T [T(t) - 20]\} I^2(t), \qquad (1)$$

where $R_{el_{20}}$ is the electrical resistance per unit length at 20 °C, $\alpha_T$ is the resistance corrective factor for variations in temperature, $I(t)$ is the cable load, and $T(t)$ is the conductor absolute temperature in °C. All but one of the remaining parameters of the equivalent network can be easily calculated according to [22].

However, the estimation of the thermal capacitance of the surrounding soil ($Q_4$) is a challenging issue that still is discussed in the relevant literature [17].

[3]Neglecting dielectric losses is practically reasonable in distribution networks. Indeed, according to the usual limits on the phase-to-ground voltages above which dielectric losses must be considered [21], it is necessary to include these losses only in few cases in MV grids.

Among the practical solutions proposed in literature, we follow the approach presented in [21] and [22] that relies on the decoupling of the network in Figure 3, in order to separately estimate the temperature rise in the internal and in the external parts of the cable. More in details, the conductor absolute temperature $T(t)$ is the sum of three contributions: i) the absolute temperature $T_S(t, z_b)$ of the soil at the burial depth $z_b$; ii) the temperature rise $\Delta T_e(t)$ of the cable external surface upon the temperature of the soil, multiplied by the attainment factor $\alpha(t)$; and iii) the temperature rise $\Delta T_i(t)$ of the conductor upon the temperature of the cable external surface:

$$T(t) = T_S(t, z_b) + \alpha(t)\, \Delta T_e(t) + \Delta T_i(t). \qquad (2)$$

Note that the attainment factor $\alpha(t)$ takes into account the interaction between the cable internal thermal transient and the cable external thermal transient. The reader is referred to [21]–[23] for the definition and for further details.

The internal temperature rise $\Delta T_i(t)$ is evaluated by superimposing the dynamic responses of the equivalent internal network to the electrical loss step variations $\Delta W_c(t_l) = W_c(t_l) - W_c(t_{l-1})$:

$$\Delta T_i(t) = \sum_{l=1}^{kF} \begin{cases} 0 & \text{if } t < t_l \\ \Delta W_c(t_l) \left[A\left(1 - e^{a(t_l - t)}\right) \right. & \\ \qquad \left. + B\left(1 - e^{b(t_l - t)}\right)\right] & \text{if } t \geq t_l, \end{cases} \qquad (3)$$

where $A, B, a, b$ are the parameters of an equivalent two-loop circuit obtained from thermal resistances and thermal capacitances $R_1, R_3, Q_0, Q_1, Q_2, Q_3$ [21].

Similarly, the external temperature rise $\Delta T_e(t)$ is evaluated by superimposing the dynamic responses of the equivalent external network to the electrical loss step variations:

$$\Delta T_e(t) = \sum_{l=1}^{kF} \begin{cases} 0 & \text{if } t < t_l \\ \Delta W_c(t_l) \dfrac{\rho_T(t, z_b)}{4\pi} \cdot & \\ \cdot \left[ \mathrm{Ei}\left( \dfrac{-z_b^2}{\delta_T(t, z_b) \cdot (t - t_l)} \right) \right. & \\ \qquad \left. - \mathrm{Ei}\left( \dfrac{-D_e^2}{16 \delta_T(t, z_b) \cdot (t - t_l)} \right) \right] & \text{if } t \geq t_l \end{cases} \qquad (4)$$

where $\mathrm{Ei}(\cdot)$ is the exponential integral function, $\rho_T(t, z_b)$ is the thermal resistivity of the soil at the burial depth, and $\delta_T(t, z_b)$ is the thermal diffusivity of the soil at the burial depth. The dynamics of the soil thermal characteristics (i.e., $\rho_T(t, z_b)$ and $\delta_T(t, z_b)$ in (4) and $T_S(t, z_b)$ in (2)) are not easily estimated, and the thermal-hydraulic model of the soil described in the following sub-Section is used in order to catch significant variations due to environmental time-varying conditions.

The cable-soil model in (1)-(4) is used in an inverse form in the PSM proposed in this paper: the conductor absolute

temperature $T(t_{(k-1)F+1}), \ldots T(t_{kF})$ during each sub-interval of the time horizon is set at the target operating temperature $T^*$, and we solve the equations for the cable load $I(t)$, thus returning $F$ forecasts $\hat{I}^*_{t_{(k-1)F+1}}, \ldots, \hat{I}^*_{t_{kF}}$ of UGC DLR, one for each sub-interval. Eventually, the comprehensive forecast of the UGC DLR $\hat{I}^*_h$ is conservatively extracted as the minimum value among them:

$$\hat{I}^*_h = \min\left\{\hat{I}^*_{t_{(k-1)F+1}}, \ldots, \hat{I}^*_{t_{kF}}\right\}, \tag{5}$$

or less conservatively as a thermally-equivalent averaged value:

$$\hat{I}^*_h = \sqrt{\frac{1}{F}\sum_{l=1}^{F}\left(\hat{I}^*_{t_{(k-1)F+l}}\right)^2}. \tag{6}$$

### 2) EVALUATION OF THE SOIL THERMAL-HYDRAULIC DYNAMICS

In order to predict the UGC DLR, it is necessary to obtain forecasts of the following three environmental variables: the soil temperature $T_S(t, z_b)$ at the burial depth, the soil thermal resistivity $\rho_T(t, z_b)$ at the burial depth, and the soil thermal diffusivity $\delta_T(t, z_b)$ at the burial depth.

A thermal-hydraulic model is used to capture the dynamics of these thermal parameters of the soil. Indeed, as it is shown in the following, the soil thermal parameters $T_S(t, z_b)$, $\rho_T(t, z_b)$ and $\delta_T(t, z_b)$ strongly depend on the moisture content of the soil, thus requiring to address also the hydraulic dynamics (in terms of soil moisture content). Note that the moisture migration caused by the heating of the zones in close proximity to the cable is not considered in this paper, and it will be investigated in future works.

In order to correctly address both the thermal and the hydraulic dynamics, suitable time resolution must be selected. Indeed, a 1-hour time discretization appears not to be adequate; therefore, we selected a 5-minutes (sub-hourly) time discretization to solve the dynamic thermal-hydraulic model described in the following.

External forcing inputs (i.e., weather parameters) drive the dynamics of the three required environmental variables. These inputs are needed throughout the entire forecast lead time; however, in order to avoid a redundant and unnecessarily-burdensome forecasting system, the external forcing inputs are forecasted at a hourly time resolution.

The thermal-hydraulic model is described in the following sub-Sections.

#### *a: Modeling the soil thermal diffusivity*

The soil thermal diffusivity is estimated through the regression model developed in [24][4]:

$$\delta_T(t, z) = -14.8 + 0.209N + 4.79\theta(t, z), \tag{7}$$

[4]The regression coefficients in (7) have been estimated in [24] to fit both a sandy and a clay soil, returning good fitting performances in both analyses. In order to further improve the results, these coefficients should be estimated from field experiments on the specific soil considered for the cable burial, whenever it is possible.

where $N$ is the soil composition (it is a fixed term, since it is the mass of sand and clay particles, in percentage of the total mass), and $\theta(t, z)$ is the soil moisture content (i.e., the ratio of the volume of water to the total volume of soil). Therefore, an accurate assessment of the hydraulic dynamics is mandatory in order to catch the variations in soil thermal diffusivity.

#### *b: Modeling the soil thermal resistivity*

The soil thermal resistivity is linked to the soil thermal diffusivity $\delta_T(t, z)$, to the soil specific heat $C_{ST}(t, z)$, and to the dry-soil density $\sigma_{S,dry}$ (i.e., the mass-volume ratio of the soil at the residual moisture content $\theta_{res}$) using the following formula:

$$\rho_T(t, z) = \frac{1}{\delta_T(t, z)\cdot\sigma_{S,dry}\cdot C_{ST}(t, z)}. \tag{8}$$

The dry-soil density is a known parameter once the type of soil is fixed, and can reasonably be assumed to be time-invariant.

The soil specific heat is instead obtained from the soil volumetric heat capacity $CV_{ST}(t, z)$ and from the moist-soil density $\sigma_S(t, z)$:

$$C_{ST}(t, z) = \frac{CV_{ST}(t, z)}{\sigma_S(t, z)}; \tag{9}$$

the first is estimated through the regression model developed in [24]:

$$CV_{ST}(t, z) = -0.224 - 0.00561N + 0.753\sigma_{S,dry} + 5.81\theta(t, z), \tag{10}$$

whereas the latter is the dry-soil density, adjusted for the soil moisture content:

$$\sigma_S(t, z) = \sigma_{S,dry}\left[1 + \theta(t, z)\right]. \tag{11}$$

In practice, the soil thermal resistivity is a direct function of the soil moisture content, once the time-invariant soil composition and dry-soil density are assigned, given the soil type. Therefore, an accurate assessment of the hydraulic dynamics is mandatory in order to catch the variations in soil thermal resistivity.

#### *c: Modeling the soil temperature*

The dynamics of soil temperature $T_S(t, z)$ are modeled through the well-known Fourier law [25]:

$$\frac{\partial T_S(t, z)}{\partial t} = \frac{\partial}{\partial z}\left[\delta_T(t, z)\frac{\partial T_S(t, z)}{\partial z}\right], \tag{12}$$

that is a spatial-temporal differential equation with non-constant coefficients (i.e., the soil thermal diffusivity). It can be solved by means of finite-elements methods, or by means of numerical algorithms. In this paper, we use the latter approach based on finite differences, that requires to initialize the problem giving boundary and initial conditions.

In practice, boundary conditions $T_S(t, z_1)$ at the upper layer are set at the SVR soil temperature forecasts $\hat{T}_S(t, z_1)$,

whereas boundary conditions $T_S(t, z_L)$ at the lower layer are set at a reference temperature of water tables [16].

The initial conditions $T_S(t_1, z)$ in the whole soil column are set by means of a linear interpolation between the soil temperature at the upper layer measured at the forecast start time and the reference temperature of the water table.

*d: Modeling the soil moisture content*

As discussed above, the soil thermal diffusion, the soil thermal resistivity, and the soil temperature depend on the soil moisture content. The soil hydraulic dynamics are captured by [26]:

$$\frac{\partial\theta(t,z)}{\partial t} = \frac{\partial}{\partial z}\left[\delta_\theta(t,z)\frac{\partial\theta(t,z)}{\partial z} + k_\theta(t,z)\right], \tag{13}$$

where $\delta_\theta(t, z)$ is the soil hydraulic diffusivity and $k_\theta(t, z)$ is the soil hydraulic conductivity (also called hydraulic permeability). Solving this equation is not a trivial task, since both the non-constant parameters of the spatial-temporal differential equation (13) depend on the soil moisture content. The soil hydraulic diffusivity and the soil hydraulic conductivity are, respectively [27]:

$$\delta_\theta(t,z) = \frac{(1-m_{vg})\,k_{sat}}{\alpha_{vg}\cdot m_{vg}\,(\theta_{sat}-\theta_{res})}\cdot[\Theta(t,z)]^{\left(0.5-\frac{1}{m_{vg}}\right)} \cdot\left\{\frac{1}{\left[1-[\Theta(t,z)]^{\frac{1}{m_{vg}}}\right]^{m_{vg}}} + \left[1-[\Theta(t,z)]^{\frac{1}{m_{vg}}}\right]^{m_{vg}} - 2\right\}, \tag{14}$$

$$k_\theta(t,z) = k_{sat}\sqrt{\Theta(t,z)}\left\{1-\left[1-[\Theta(t,z)]^{\frac{1}{m_{vg}}}\right]^{m_{vg}}\right\}^2, \tag{15}$$

where $\theta_{sat}$ is the saturated-soil moisture content, $k_{sat}$ is the saturated-soil hydraulic conductivity, and $\alpha_{vg}, m_{vg}$ are van Genuchten coefficients [27]. Note that $\Theta(t, z)$ is the normalized soil moisture content (ranging from 0 to 1, for dry soil and saturated soil, respectively); it is obtained as:

$$\Theta(t,z) = \frac{\theta(t,z)-\theta_{res}}{\theta_{sat}-\theta_{res}}. \tag{16}$$

To tackle the problem, the solution of (13) is obtained through a numerical approach based on finite differences.

Boundary conditions $\theta(t, z_1)$ at the upper layer are set at a value that depends on the SVR soil precipitation forecasts $\hat{r}_{h-k+1}, \ldots, \hat{r}_h$; indeed, the dynamics of water diffusion through the soil column are captured by the following equation [28]:

$$\frac{d\theta(t,z_1)}{dt} = -\frac{V}{\theta_{sat}z_{root}}\theta(t,z_1) + \frac{1-\Phi}{\theta_{sat}z_{root}}\hat{r}(t) \tag{17}$$

where constant parameters $V$, $1-\Phi$, and $z_{root}$ are respectively the soil water loss coefficient, the net rain coefficient, and the vegetation root depth [29]. Boundary conditions $\theta(t, z_L)$ at the lower layer are instead set at the saturated-soil moisture content $\theta_{sat}$.

The initial conditions $\theta(t_1, z)$ in the whole soil column are set by means of a linear interpolation between the soil moisture content at the upper layer estimated from precipitation measurements at the forecast start time and the saturated-soil moisture content.

### 3) FORECASTING SOIL TEMPERATURE AT THE UPPER LAYER, PRECIPITATION, AND CABLE LOAD

Forecasts of soil temperature at the upper layer, precipitation, and cable load are needed as inputs of the models presented in the previous sub-Sections. In this paper, we use SVR-based approaches for the PSM, in order to satisfy this need.

SVR models link the soil temperature $T_{S,h}(z_1)$ at the upper layer, the precipitation $r_h$, and the cable load $I_h$ to informative predictor variables, selected among past measurements of the same variables (endogenous predictors) and other variables (exogenous predictors). To avoid a verbose presentation, SVR model is formulated in this sub-Section for the generic variable $y_h$, that may represent the soil temperature, precipitation, or cable load.

Let $\mathbf{X}_h = \{x_{h_1}, x_{h_2}, \ldots, x_{h_m}\}$ be a vector of $m$ informative predictor variables (endogenous and exogenous ones). The generic SVR model is [30]:

$$\hat{y}_h = \langle\boldsymbol{\beta}, \boldsymbol{X}_h\rangle + \beta_0, \tag{18}$$

where $\beta_0$ and $\boldsymbol{\beta} = \beta_1, \ldots, \beta_m$ are the parameters of the model, and the notation $\langle\cdot,\cdot\rangle$ indicates a linear (or nonlinear) function of predictors and parameters.[5] Model parameters can be estimated given a historic data vector $\boldsymbol{Y}_h = \{y_{h-k-M}, \ldots, y_{h-k}\}$ of $M+1$ measurements of the target variable, and $M+1$ vectors $\boldsymbol{X}_{h-k-M}, \ldots, \boldsymbol{X}_{h-k}$, each made of $m$ predictors, all available at the forecast start time $h-k$. Assigning an arbitrary threshold $\tau$, the SVR problem consists in the constrained minimization of the sum of the norm $\frac{1}{2}\|\boldsymbol{\beta}\|^2$ and of auxiliary parameters $\boldsymbol{\xi} = \{\xi_0, \xi_1, \ldots, \xi_M$, $\boldsymbol{\xi}^* = \{\xi_0^*, \xi_1^*, \ldots, \xi_M^*$, specifically introduced for the SVR problem; its formulation is:

$$\begin{aligned}
&\hat{\boldsymbol{\beta}}, \hat{\beta}_0, \hat{\boldsymbol{\xi}}, \hat{\boldsymbol{\xi}}^* \\
&= \operatorname{argmin}_{\boldsymbol{\beta},\beta_0}\frac{1}{2}\|\boldsymbol{\beta}\|^2 + L_C\sum\nolimits_{i=0}^{M}(\xi_i+\xi_i^*), \\
&\quad \text{s.t.} \\
&\qquad y_{h-k-i} - \langle\boldsymbol{\beta}, \boldsymbol{X}_{h-k-i}\rangle - \beta_0 \le \tau + \xi_i \quad \forall i = 0,\ldots,M, \\
&\qquad \langle\boldsymbol{\beta}, \boldsymbol{X}_{h-k-i}\rangle + \beta_0 - y_{h-k-i} \le \tau + \xi_i^* \quad \forall i = 0,\ldots,M, \\
&\qquad \xi_i, \xi_i^* \ge 0 \quad \forall i = 0,\ldots,M,
\end{aligned} \tag{19}$$

where $L_C$ is an assigned loss coefficient that negatively weights estimated values that differ from the actual value by

[5] In the linear case, the function $\langle$ indicates the scalar product; nonlinear relationships may instead be modeled through kernel functions [30].

more than $\tau$. The Lagrange problem linked to (18) is:

$$\begin{aligned}&\hat{\boldsymbol{\lambda}}, \hat{\boldsymbol{\lambda}}^{*}\\ &= \operatorname{argmin}_{\boldsymbol{\lambda},\boldsymbol{\lambda}^{*}} \sum_{i=0}^{M} y_i \left(\lambda_i - \lambda_i^{*}\right) - \tau \sum_{i=0}^{M} \left(\lambda_i^{*} + \lambda_i\right) + \\ &\quad - \frac{1}{2} \sum_{i=0}^{M} \sum_{j=0}^{M} \left(\lambda_i - \lambda_i^{*}\right) \left(\lambda_j - \lambda_j^{*}\right) \langle \boldsymbol{X}_{h-k-i}, \boldsymbol{X}_{h-k-i} \rangle \\ &\quad \text{s.t.} \\ &\qquad \sum_{i=0}^{M} \left(\lambda_i^{*} - \lambda_i\right) = 0, \\ &\qquad 0 \le \lambda_i \le L_C \quad \forall i = 0, \ldots, M, \\ &\qquad 0 \le \lambda_i^{*} \le L_C \quad \forall i = 0, \ldots, M, \end{aligned} \tag{20}$$

where $\boldsymbol{\lambda} = \{\lambda_0, \ldots, \lambda_M\}$ and $\boldsymbol{\lambda}^{*} = \{\lambda_0^{*}, \ldots, \lambda_M^{*}\}$ are the Lagrange coefficients. Once the problem (20) is solved, the original SVR coefficients can be then expressed as:

$$\hat{\beta}_j = \sum_{i=0}^{M} \left(\hat{\lambda}_i - \hat{\lambda}_i^{*}\right) x_{h-k-i_j} \qquad \forall j = 1, \ldots, m, \tag{21}$$

so that the target variable is forecasted as:

$$y_h = \sum_{i=0}^{M} \left(\hat{\lambda}_i - \hat{\lambda}_i^{*}\right) \langle \boldsymbol{X_i}, \boldsymbol{X_h} \rangle + \hat{\beta}_0, \tag{22}$$

where $\hat{\beta}_0$ is estimated through the Karush-Kuhn-Tucker constraints:

$$\begin{aligned}\hat{\beta}_0 &= y_{h-k-i} - \langle \boldsymbol{\beta}, \boldsymbol{X_{h-k-i}} \rangle - \tau \quad \text{if } 0 \le \hat{\lambda}_i \le L_C \\ \hat{\beta}_0 &= y_{h-k-i} - \langle \boldsymbol{\beta}, \boldsymbol{X_{h-k-i}} \rangle + \tau \quad \text{if } 0 \le \hat{\lambda}_i^{*} \le L_C. \end{aligned} \tag{23}$$

### B. DATA-DRIVEN UGC DLR FORECASTING METHOD

A data-driven approach is tested for both the intraday and the day-ahead scenarios. This approach is developed following approaches already developed for OHL DLR forecasting [19], [20].

The data-driven approach can be summarized as it follows: calling $y_h$ the target variable to forecast at horizon $h$, and $\boldsymbol{X}_h$ the array of predictors (known information at the forecast origin $h-k$), it is necessary to identify a function $f$ so that:

$$y_h = f(\boldsymbol{X}_h). \tag{24}$$

The function $f$, the forecast model, can be parametric or non-parametric. In the first case, the number of parameters used to fit the model is finite, as in the case of a Linear Regression (LR). In the second case, the model can be grown to include an infinite number of parameters, as in the case of decision trees and random forests. In this paper we explore both cases: LR is selected for its simplicity of use and for comparison purposes, whereas Random Forest Regression (RFR) is selected since it is best suited to deal with problems characterized by a large number of data, and it has been proven to be successful for the forecast of OHL DLR [19], in which RFR has been identified as the model with the best performance [31]. The two cases are denoted as DDM-LR and DDM-RFR, respectively.

#### 1) RANDOM FOREST REGRESSION

RFR is a machine-learning method in which the model is composed by $K_d$ decisional trees, each of which gives an estimation of the output parameter. During the training phase, each node is split using a random selection of features, whereas during the forecasting phase each tree is sampled with the same distribution of input. The output of the model for a forecast is then a set of $K_d$ values, and the mean of the outputs of the trees is chosen as the result for a deterministic forecast. A schematic description of the process is presented in Figure 4.

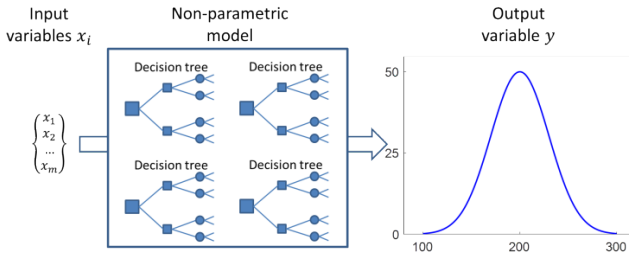


**FIGURE 4.** Random forest regression.

Several aspects of this model are important to understand the rest of the study and the analysis of the results. Firstly, being based on decision trees trained on a past dataset, the model is not able to predict situations that have not already been observed. Secondly, this model is less sensitive to the problem size and can achieve good performances also with large datasets. Finally, the model can give useful information about the relative importance of each input used, thanks to the analysis of the frequency at what each input is found in the explanatory values of the trees.

In this paper, the RFR is used for forecasting the UGC DLR, as described and calculated in Section III.A.1, with horizons spanning from 1 to 36 hours. Therefore the output of the forecast model $y_h$ in (23) is the rating $\hat{I}_h^{*}$ from (6), calculated using the historical weather condition data described in Section IV.B. Regarding the explanatory variables, the following features are selected for the study, as they can be divided between observed variables (relative to the forecast origin $h-k$) or forecasted variables (known at the forecast origin $h-k$, but relative to time horizon $h$).

Among the observed variables, we select:

- weekday and hour. They respectively represent the day of the week and the hour of the day of the forecast horizon h. They are selected since the UGC DLR depends also on the load recent history, and this is heavily dependent on human activities characterized by weekly and daily cycles;
- last estimated UGC DLR $\hat{I}_{h-k}^{*}$ and last homologous UGC DLR ($\hat{I}_{h-24}^{*}$ or $\hat{I}_{h-48}^{*}$). These are the conductor rating at the forecast origin, and the rating estimated one or two days before the forecast horizon (chosen whether the lead time is smaller or greater than 24 hours). These values are both calculated as in (6);

they are investigated because of the high inertia of the cable-soil system, and they are expected to be important explanatory variables short lead times;
- last measured ambient temperature $T_{s,h-k}(z_1)$, precipitation $r_{h-k}$, and load $I_{h-k}$, and last homologous ambient temperature ($T_{s,h-24}(z_1)$ or $T_{s,h-48}(z_1)$), precipitation ($r_{h-24}$ or $r_{h-48}$), and load ($I_{h-24}$ or $I_{h-48}$).

On the other hand, the forecast variables are:

- forecasts of ambient temperature (2T) and precipitation (LSP). These parameters are expected to influence the UGC DLR in two ways: firstly they influence the heat exchange with the soil (and, hence, the soil temperature profile), and secondly, they influence human activities related to the electric load. Note that the precipitation influences also the soil water content profile;
- soil temperature NWPs at different depths (SKT, STL1, STL2, STL3, STL4). These parameters influence directly the cable rating, according to its burial depth. In this paper we consider the temperature at five levels, from the soil surface down to the water table;
- soil water content NWPs at different depths (SWVL1, SWVL2, SWVL3, SWVL4). Also these parameters affect the UGC DLR according to its burial depth. Four levels are considered in this paper.

Regarding the forecast models, we choose to create a different model for each forecast horizon. This is done because it is expected that, because of thermal inertia, short-term and long-term forecasts are relatively different problems with different dynamics. We expect the frontier between these two models to lie in the region of a multiple of the time constant of the system (e.g., 3, 6 or 9 hours), but there are no empirical reasons to choose a fixed horizon beyond which starting to apply the day-ahead forecast module. On the contrary, the transient region is expected to be blurred, thus requiring individual models.

#### 2) LINEAR REGRESSION

In order to evaluate the benefit arising from the use of a complex model such as the random forest, its performance will be compared with a simpler LR model, which can be expressed as in:

$$y_h = \sum_{i=1}^{m} \alpha_i \cdot x_{h_i}, \tag{25}$$

where $\alpha_1, \ldots, \alpha_m$ are the coefficients of the LR model, and $x_{h_1}, \ldots, x_{h_m}$ are the $m$ predictors of the models. As in the SVR case, the coefficients are estimated in the training step of the procedure; for LR, they are obtained through the ordinary least square approach.

Since the LR model is sensitive to the number of inputs, it quickly reduces its performances as the number of inputs increases; therefore it is trained in this paper on a reduced set of features, namely: the last estimated UGC DLR $\hat{I}^*_{h-k}$, soil temperature NWPs at the cable burial depth (STL3), and soil volumetric water content NWPs at the cable burial depth (SWVL3).

## IV. CASE STUDY BACKGROUND

The UGC DLR forecasting methods are applied to actual data in order to produce intraday and day-ahead forecasts for three months. Details on the considered setup, on the cable-soil system, and on the environmental framework are briefly presented in this Section.

### A. HYPOTHESES ON THE TYPE OF SOILS AND CABLE

Two different soils are considered, in order to assess the performances of the method under different conditions. A sandy soil and a clay soil are indeed considered in the applications; they are usually selected in UGC DLR applications since their performances are antipodal. Also, sandy soils are very representative of backfilling materials, in which cables are often buried due to their advantageous thermal characteristics. Table 1 reports the soil parameters used in the numerical applications; they are taken from the typical values reported in a comprehensive soil database [32].

The specifics of the copper three-core, LV cable considered in the numerical applications are instead provided by the manufacturers and are reported in Table 2. The cable is considered directly buried in clay or sandy soil. The cable insulation is made of EPR, and the cable sheath is made of polychloroprene.

**TABLE 1. Clay and sandy soils parameters used in the numerical applications.**

| Parameter | Symbol | Units | Clay soil | Sandy soil |
|---|---|---|---|---|
| Dry-soil density | $\sigma_{S,dry}$ | g/cm$^3$ | 1.2 | 1.51 |
| Lower layer | $z_L$ | m | 4.9 | 4.9 |
| Net rain coefficient | $1-\Phi$ | - | 0.95 | 0.95 |
| Residual moisture content | $\theta_{res}$ | - | 0.102 | 0.058 |
| Saturated-soil hydraulic conductivity | $k_{sat}$ | cm/day | 17.3 | 203.7 |
| Saturated-soil moisture content | $\theta_{sat}$ | - | 0.46 | 0.37 |
| Soil composition | $N$ | % | 100 | 100 |
| Soil temperature at the lower layer | $T_S(t, z_L)$ | °C | 5 | 5 |
| Upper layer | $z_1$ | m | 0.1 | 0.1 |
| van Genuchten coefficient | $\alpha_{vg}$ | cm$^{-1}$ | 0.021 | 0.035 |
| van Genuchten coefficient | $m_{vg}$ | - | 1.20 | 3.19 |
| Water loss coefficient | $V$ | cm/day | 1.6 | 1.6 |

### B. MEASURED WEATHER PARAMETERS

The available weather data is measured at Camborne (UK) (Lat. 50.2178, Lon. -5.3266); the dataset has been made publically available by the Centre for Environmental Data Analysis [33]. In the following case studies, the soil temperature at 10 centimeters depth and the precipitation are collected with hourly frequency from January 1$^{st}$ 2016 to December 31$^{st}$ 2016, thus 8784 measurements for each variable are available.

Cable loads are measured with hourly frequency during the same time interval at an industrial factory in which

**TABLE 2. Cable parameters used in the numerical applications.**

| Parameter | Symbol (if appearing) | Units | Value |
|---|---|---|---|
| Burial depth | $z_b$ | m | 0.7 |
| Copper volumetric specific heat | - | MJ/m$^3$·K | 3.78 |
| Electrical resistance per unit length at 20 °C | $R_{el_{20}}$ | mΩ/m | 0.727 |
| External diameter of the conductors | - | mm | 6.39 |
| External diameter of the insulation | - | mm | 9.24 |
| External diameter of the sheath | - | mm | 30.51 |
| Geometric factor | - | - | 0.91 |
| Insulation thermal resistivity | - | m·K/W | 3.5 |
| Insulation volumetric specific heat | - | MJ/m$^3$·K | 2.00 |
| Internal diameter of the sheath | - | mm | 22.31 |
| Rated current | - | A | 142 |
| Resistance corrective factor for variations in temperature | $\alpha_T$ | K$^{-1}$ | $3.93 \cdot 10^{-3}$ |
| Conductor section | - | mm$^2$ | 25 |
| Sheath thermal resistivity | - | m·K/W | 5.5 |
| Sheath volumetric specific heat | - | MJ/m$^3$·K | 2.00 |
| Target operating temperature | $T^*$ | °C | 85 |

distribution transformers are manufactured. The cable loads do not show any weather correlation throughout the whole year; this is a thoughtful choice, in order to validate the proposed method under no specific assumption on the cable loading that could enhance or diminish the impact of weather conditions upon the UGC DLR.

Statistical parameters of the three considered datasets are reported in Table 3.

**TABLE 3. Statistical parameters of the soil temperature, precipitation, and cable load during the year 2016.**

| Parameter | Dataset | | |
|---|---|---|---|
| | Soil temperature | Precipitation | Cable load |
| Units | °C | mm/h | A |
| Min | 2.30 | 0.00 | 29.82 |
| Mean | 12.26 | 0.13 | 106.98 |
| Median | 11.40 | 0.00 | 114.36 |
| Max | 29.80 | 11.40 | 194.73 |
| Standard deviation | 5.15 | 0.52 | 36.85 |

### C. FORECASTED WEATHER PARAMETERS

Historical weather forecasts are obtained from the European Center for Middle-range Weather Forecast (ECMWF) [34]; they are made of day-ahead point forecasts for the location of Camborne (UK) from January 1$^{st}$ 2016 to December 31$^{st}$ 2016. The forecasts used in this study are briefly presented in Table 4. They are all relative to the noon run, and the forecast horizons span from 1 to 36 hours.

## V. RESULT AND DISCUSSION

Results of intraday and day-ahead UGC DLR forecasts are presented separately, for the last three months of the year 2016. The first nine months are indeed used to train the SVR model, whilst six months are used to train the RFR and LR forecasting model. Results are compared to those obtained through the Persistence Method (PM), i.e., variables are assumed constant throughout the forecast lead time. A 5-minutes time discretization is used in all of the considered applications (thus, $F = 12$).

**TABLE 4. Description of the numerical weather predictions.**

| Symbol | Unit | Description |
|---|---|---|
| 2T | K | Air temperature at 2 meters from the ground |
| LSP | m·m$^{-2}$ | Precipitation |
| SKT | K | Soil skin temperature or radiative surface temperature |
| STL1 | K | Top soil temperature, 1-7 cm |
| STL2 | K | Deep soil temperature, 7-28 cm |
| STL3 | K | Climatological deep soil temperature, 28-100 cm |
| STL4 | K | Soil fourth layer temperature 100-289 cm |
| SWVL1 | m$^3$·m$^{-3}$ | Top soil volumetric water content, 1-7 cm |
| SWVL2 | m$^3$·m$^{-3}$ | Deep soil volumetric water content, 7-28 cm |
| SWVL3 | m$^3$·m$^{-3}$ | Climatological deep soil volumetric water content, 28-100 cm |
| SWVL4 | m$^3$·m$^{-3}$ | Soil fourth layer volumetric water content, 100-289 cm |

### A. INTRADAY UGC DLR FORECAST

Results of the intraday UGC DLR forecast are presented in this sub-Section.

In order to carefully assess the overall quality of PSM forecasts, we first analyze the results of the SVR forecasts of soil temperature, precipitation, and load current throughout the intraday forecast lead times (i.e., from 1 to 12 hours ahead), which are afterwards used as inputs of the PSM. Results are presented in terms of Mean Absolute Errors (MAEs) and Normalized MAEs (NMAEs) in Table 5, with a comparison to the results of the PM. Results are averaged during the last three months of the year 2016; the normalization term is the maximum value registered for each variable during the three months (17.00 °C, 5.60 mm/h, and 173.22 A for soil temperature, precipitation, and cable load, respectively). Soil temperature and cable load forecast errors increase with the lead time, whereas precipitation forecast errors remain practically constant as the lead time increases. In all cases, SVR forecasts return errors smaller than the PM ones.

Feeding the thermal-hydraulic model of the cable-soil system with input SVR forecasts, we obtain forecasts of the soil thermal resistivity, of the soil temperature at the cable burial depth, and of the soil thermal diffusivity. The corresponding NMAEs are reported in Table 6 for clay and sandy soils; errors are calculated with respect to the values obtained by feeding the actual weather data to the thermal-hydraulic model. The normalizing values are the maximum registered values of soil thermal resistivity, soil temperature, and soil thermal diffusivity at the burial depth, which are respectively 0.85 m · K/W, 11.43 °C, and $3.05 \cdot 10^{-7}$ m/s$^2$ in the case of clay soil, and 0.75 m · K/W, 11.71 °C, and $6.80 \cdot 10^{-7}$ m/s$^2$ in the case of sandy soil.

**TABLE 5.** SVR forecasting errors of the psm inputs (soil temperature at the upper layer, precipitation, and cable load).

| Variable | Error index | Forecast lead time $k$ | | | | | | | | | | | |
|---|---|---|---|---|---|---|---|---|---|---|---|---|---|
| | | 1 | 2 | 3 | 4 | 5 | 6 | 7 | 8 | 9 | 10 | 11 | 12 |
| Soil temperature at the upper layer | SVR MAE [°C] | 0.19 | 0.40 | 0.61 | 0.80 | 0.99 | 1.16 | 1.32 | 1.47 | 1.61 | 1.73 | 1.85 | 1.95 |
| | SVR NMAE [%] | 1.15 | 2.36 | 3.57 | 4.72 | 5.80 | 6.83 | 7.77 | 8.65 | 9.45 | 10.20 | 10.86 | 11.46 |
| | PM MAE [°C] | 0.23 | 0.44 | 0.64 | 0.81 | 0.97 | 1.10 | 1.21 | 1.30 | 1.37 | 1.42 | 1.46 | 1.49 |
| | PM NMAE [%] | 1.34 | 2.60 | 3.75 | 4.79 | 5.69 | 6.46 | 7.11 | 7.64 | 8.06 | 8.37 | 8.59 | 8.75 |
| Precipitation | SVR MAE [mm/h] | 0.10 | 0.11 | 0.11 | 0.11 | 0.11 | 0.11 | 0.11 | 0.11 | 0.11 | 0.11 | 0.11 | 0.11 |
| | SVR NMAE [%] | 1.78 | 1.98 | 2.05 | 2.06 | 2.06 | 2.06 | 2.06 | 2.05 | 2.05 | 2.05 | 2.05 | 2.05 |
| | PM MAE [mm/h] | 0.11 | 0.14 | 0.15 | 0.16 | 0.17 | 0.18 | 0.18 | 0.19 | 0.19 | 0.19 | 0.19 | 0.20 |
| | PM NMAE [%] | 1.97 | 2.59 | 2.74 | 2.88 | 3.10 | 3.24 | 3.30 | 3.43 | 3.47 | 3.47 | 3.40 | 3.53 |
| Cable load | SVR MAE [A] | 5.40 | 7.91 | 9.59 | 10.92 | 12.05 | 13.12 | 13.93 | 14.66 | 15.19 | 15.57 | 15.91 | 16.20 |
| | SVR NMAE [%] | 3.12 | 4.57 | 5.54 | 6.30 | 6.86 | 7.57 | 8.04 | 8.47 | 8.77 | 8.99 | 9.18 | 9.35 |
| | PM MAE [A] | 6.65 | 10.27 | 13.51 | 16.23 | 18.76 | 21.23 | 23.62 | 25.94 | 27.60 | 28.89 | 29.74 | 30.50 |
| | PM NMAE [%] | 3.84 | 5.93 | 7.80 | 9.37 | 10.83 | 12.26 | 13.64 | 14.97 | 15.93 | 16.62 | 17.17 | 17.61 |

**TABLE 6.** Intraday normalized mean absolute errors of intermediate soil parameters in the psm (soil thermal resistivity, soil temperature at the cable burial depth, and soil thermal diffusivity) for sandy and clay soils.

| Variable | Units | Type of soil | Normalized Mean Absolute Errors | | | | | | | | | | | |
|---|---|---|---|---|---|---|---|---|---|---|---|---|---|---|
| | | | Forecast lead time $k$ | | | | | | | | | | | |
| | | | 1 | 2 | 3 | 4 | 5 | 6 | 7 | 8 | 9 | 10 | 11 | 12 |
| Soil thermal resistivity | [%] | Clay | 0.00 | 0.51 | 1.01 | 1.52 | 2.03 | 2.54 | 3.06 | 3.57 | 4.08 | 4.59 | 5.10 | 5.61 |
| | | Sand | 0.01 | 0.68 | 1.37 | 2.09 | 2.83 | 3.57 | 4.32 | 5.07 | 5.83 | 6.59 | 7.35 | 8.12 |
| Soil temperature at the cable burial depth | $\cdot 10^{-3}$ [%] | Clay | 0.00 | 0.02 | 0.08 | 0.24 | 0.55 | 1.07 | 1.87 | 3.03 | 4.61 | 6.69 | 9.35 | 12.68 |
| | | Sand | 0.02 | 0.22 | 0.85 | 2.25 | 4.75 | 8.72 | 14.57 | 22.70 | 33.46 | 47.09 | 64.05 | 84.45 |
| Soil thermal diffusivity | [%] | Clay | 0.00 | 0.05 | 0.10 | 0.16 | 0.21 | 0.26 | 0.32 | 0.37 | 0.42 | 0.48 | 0.53 | 0.58 |
| | | Sand | 0.01 | 0.14 | 0.28 | 0.44 | 0.61 | 0.78 | 0.96 | 1.14 | 1.32 | 1.51 | 1.69 | 1.88 |

Due to the slow thermal and hydraulic dynamics of the soils, the errors for small lead times are practically unintelligible; indeed, making reasonable errors in the SVR forecasting of soil temperature at the upper layer and precipitation has practically no negative impact on estimating soil thermal parameters at small lead times. This is instead not true for greater lead times since SVR forecasting errors significantly impact the estimations of soil thermal resistivity and soil thermal diffusivity.

Note that the errors in estimating soil temperature at the cable burial depth are always unintelligible; this is an important outcome, since future works may neglect the dynamic estimation of the soil temperature at the cable burial depth, to avoid unnecessary complications.

As expected, the dynamics of clay soil is definitely slower than the dynamics of sandy soils; this can be evidenced from the smaller forecasting errors for all of the thermal characteristics of the soil.

Eventually, the results of the UGD DLR forecasts are shown in Table 7 in terms of MAEs and NMAEs for various lead times; PSM, DDM-LR, DDM-RFR, and PM results are reported in Table 7.

Errors are calculated with respect to the values obtained by feeding actual weather and cable load data to the thermal-hydraulic model of the soil and to the cable-soil thermal model. The normalizing values are the maximum registered values of DLR, which are 203.79 A and 224.17 A for clay and sandy soils, respectively. The target operating temperature is set at 85°C, as in Table 2; the thermal equivalent current in (6) is selected from the set of $F = 12$ forecasted values for each hour.

Figure 5 shows the PSM (Figure 5.a), DDM-LR (Figure 5.b), DDM-RFR (Figure 5.c), and PM (Figure 5.d) forecasts in the sandy-soil case, compared to the actual DLR, for a 12-hours lead time, in a week of the test period (November 5$^{th}$ to November 11$^{th}$ 2016). Figures 5 show that PSM seems to be able to better forecast the UGL DLR in the sandy-soil case.

### B. DAY-AHEAD UGC DLR FORECAST

We assess the performances of the DDM-LR and of the DDM-RFR day-ahead forecasts in terms of MAE and NMAE, averaged for the same 3-months test period of the intra-day case, comparing the results to the PM. We remind that PSM is too computationally intensive to be applied to day-ahead scenarios, thus no results are reported here. Figure 6 illustrates the evolution of MAE and NMAE over all the forecast lead times from 13 to 36 hours, for the conductor buried in sand (Figure 6.a) or clay (Figure 6.b).

For the conductor buried in clay, the DDM-LR returns better performances than the DDM-RFR for all of the considered lead times. For the conductor buried in sand, DDM-LR forecasts are characterized by a smaller error up to 22-24 hours; for longer lead times, the DDM-RFR errors are smaller than the DDM-LR ones.

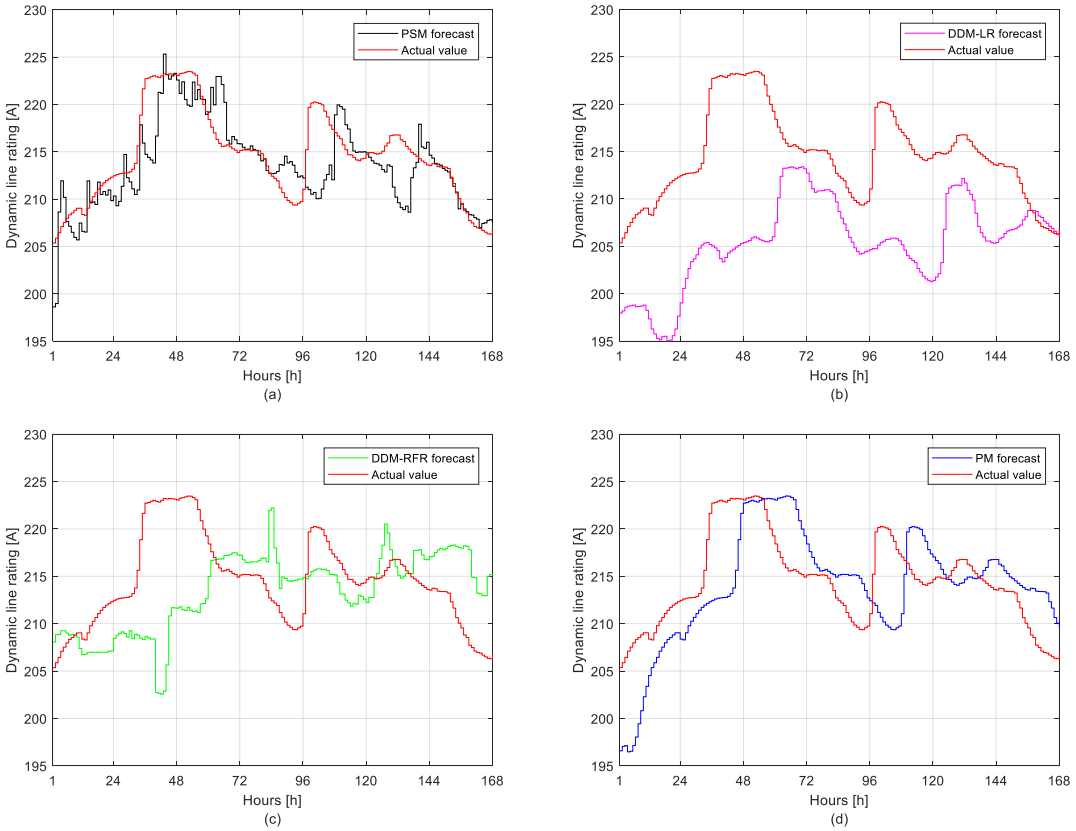


**FIGURE 5.** Dynamic line rating forecasts made through PSM (a), DDM-LR (b), DDM-RFR (c), and PM (d) for cable buried in sandy soil, made for 12-hours lead time from November 5$^{th}$to November 11$^{th}$2016.

**TABLE 7.** Intraday forecasting errors of UGC DLR in clay and sandy soils.

| Type of soil | Error index | Forecast lead time $k$ | | | | | | | | | | | |
|---|---|---|---|---|---|---|---|---|---|---|---|---|---|
| | | 1 | 2 | 3 | 4 | 5 | 6 | 7 | 8 | 9 | 10 | 11 | 12 |
| Clay | PSM MAE [A] | 0.00 | 0.24 | 0.45 | 0.64 | 0.82 | 0.98 | 1.12 | 1.26 | 1.39 | 1.50 | 1.59 | 1.67 |
| | DDM-LR MAE [A] | 1.97 | 2.57 | 3.02 | 3.34 | 3.55 | 3.65 | 3.67 | 3.65 | 3.63 | 3.64 | 3.78 | 4.07 |
| | DDM-RFR MAE [A] | 1.63 | 2.16 | 3.11 | 3.55 | 3.93 | 4.37 | 4.97 | 5.87 | 6.14 | 5.72 | 5.91 | 6.78 |
| | PM MAE [A] | 0.47 | 0.89 | 1.25 | 1.59 | 1.91 | 2.20 | 2.47 | 2.70 | 2.92 | 3.11 | 3.27 | 3.40 |
| | PSM NMAE [%] | 0.00 | 0.12 | 0.22 | 0.31 | 0.40 | 0.48 | 0.55 | 0.62 | 0.68 | 0.74 | 0.78 | 0.82 |
| | DDM-LR NMAE [%] | 0.97 | 1.26 | 1.48 | 1.64 | 1.74 | 1.79 | 1.80 | 1.79 | 1.78 | 1.79 | 1.85 | 2.00 |
| | DDM-RFR NMAE [%] | 0.80 | 1.06 | 1.52 | 1.74 | 1.93 | 2.14 | 2.44 | 2.88 | 3.01 | 2.80 | 2.90 | 3.32 |
| | PM NMAE [%] | 0.23 | 0.43 | 0.61 | 0.78 | 0.94 | 1.08 | 1.21 | 1.33 | 1.43 | 1.53 | 1.60 | 1.67 |
| Sand | PSM MAE [A] | 0.01 | 0.21 | 0.40 | 0.60 | 0.81 | 1.00 | 1.19 | 1.37 | 1.55 | 1.71 | 1.87 | 2.00 |
| | DDM-LR MAE [A] | 1.69 | 2.27 | 2.80 | 3.29 | 3.70 | 4.05 | 4.35 | 4.58 | 4.81 | 5.05 | 5.35 | 5.70 |
| | DDM-RFR MAE [A] | 2.09 | 2.70 | 3.48 | 3.97 | 4.42 | 4.50 | 4.97 | 5.24 | 5.76 | 6.08 | 6.25 | 6.59 |
| | PM MAE [A] | 0.39 | 0.75 | 1.09 | 1.41 | 1.72 | 2.01 | 2.30 | 2.56 | 2.81 | 3.05 | 3.27 | 3.48 |
| | PSM NMAE [%] | 0.01 | 0.09 | 0.18 | 0.27 | 0.36 | 0.45 | 0.53 | 0.61 | 0.69 | 0.76 | 0.83 | 0.89 |
| | DDM-LR NMAE [%] | 0.75 | 1.01 | 1.25 | 1.47 | 1.65 | 1.81 | 1.94 | 2.04 | 2.14 | 2.25 | 2.39 | 2.54 |
| | DDM-RFR NMAE [%] | 0.93 | 1.20 | 1.55 | 1.77 | 1.97 | 2.01 | 2.22 | 2.34 | 2.57 | 2.71 | 2.79 | 2.94 |
| | PM NMAE [%] | 0.18 | 0.33 | 0.48 | 0.63 | 0.77 | 0.90 | 1.02 | 1.14 | 1.25 | 1.36 | 1.46 | 1.55 |

However, the key result of the comparison is that the PM outscores both the DDM-LR and the DDM-, for all of the considered lead times. This is a very significant result of the comparison since the DDMs are directly adapted from state-of-the-art approaches on OHL DLR forecasting.

This suggests that:

- the DDM-RFR proposed is not able to correctly model the dynamic behavior of the system, since it obtains better scores than the DDM-LR only for larger lead times in the sandy-soil case, i.e., in the conditions in which the effect to the thermal inertia (and, hence, of the initial conditions) is reduced;
- compared to the PM, the DDMs based on NWPs are not a preferable solution for UGC DLR forecasting.

The main reasons behind this behavior are the significant thermal and hydraulic inertia of the surrounding soil, which,

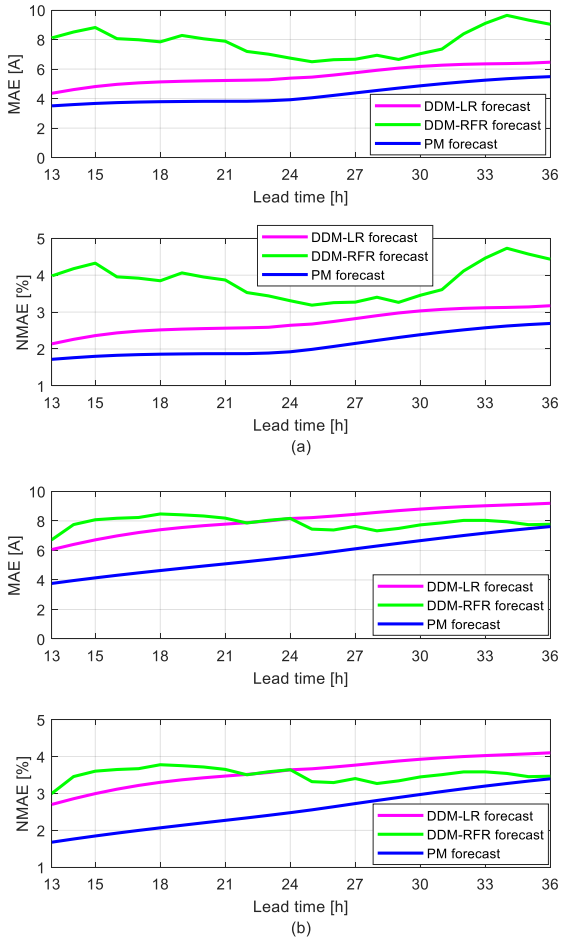


**FIGURE 6. Results of the day-ahead DDM-LR, DDM-RFR, and PM forecasts for a cable buried in clay (a) and sand(b).**

compared to the inertia of the air-filled environment considered in OHL scenarios, slow the entire UGC DLR dynamics. Indeed, in our experiments, in a range of environmental conditions that span from dry to water-saturated soils, the time constants of the surrounding soil are about few tens of hours; therefore, the UGC DLR variation from a stationary condition in intraday scenarios is mainly imposed by the cable load dynamics, whereas for larger time horizons the UGC DLR variation from a stationary condition is partially imposed by the cable load dynamics, and partially imposed by the thermal-hydraulic dynamics of the surrounding soil.

This has an enormous impact on the features selected in a DDM, thus limiting their potential effectiveness when directly applied from an OHL case. For example, this can be seen clearly from the analysis of the relative importance of the features used in the DDM-RFR for the cable buried in clay and sand, which are respectively shown in Figures 7 and 8. For the two cases, the importance of the last estimated rating $\hat{I}^*_{h-k}$ at time h-k represented in yellow in the charts, is prevalent for lead times shorter than 12 hours, and it decreases for longer lead times.

A second observation arises from the analysis of the results represented in Figures 7 and 8. For day-ahead forecast lead times (i.e., longer than 12 hours), the most important features are the forecasts of weather variables at deep soil levels, but they are different for the two cables. In the case of the cable buried in sand, the soil water content (in blue) is the most important feature, whilst for the cable in clay soil, the soil temperature (in pink) is the most important feature. This is coherent with the soil thermo-hydraulic model described in Section III.A, and with the differences occurring in the dynamics for the two types of soils.

In both cases, the weekday is also an important parameter, due to the seasonality and to the importance of the electric load in the determination of the DLR. Other features are used seldom for all the horizons, and they do not account for more than the 20% of the feature importance used by the trees of the RFR.

### C. DISCUSSION ON THE RESULTS

Several observations arise from the analysis of the data and from the comparison of different methods.

The results suggest that a dynamic model is mandatory in order to take into account the large thermal-hydraulic inertia of the cable-soil system. In fact, the performances of the DDMs and of the persistence benchmark are always poorer than the performances of the dynamic PSM, for the intraday scenario (i.e., for the lead times they have been both calculated). This is an important result since it can shape future research in several directions.

Regarding the physical modeling of the cable-soil system, the main outcome is that it shows good performances, but it lacks consistency for longer lead times. In particular, at its actual state, it is inapplicable for lead times greater than 16 hours, since the computational time would exceed the forecast lead time. This is an intrinsic feature of the method since it is based on the dynamic modeling of the cable-soil system. A further research effort in this direction would require some simplifications in the model (7)-(17), introducing only small approximations in the numerical results (e.g., future works may neglect the dynamic estimation of the soil temperature at the cable burial depth, as explained before).

Regarding the statistical forecasts, three approaches can be followed:

- firstly, it is possible to use other machine learning methods than the LR and the RFR, in order to forecast environmental conditions that could be used as input of the dynamic model, as it is done with the SVM in Section III.B;
- secondly, it is possible to develop models taking into account the evolution of the rated forecast along all the horizons in order to exploit better the information about the large thermal inertia;
- the last possibility is to combine physical and statistical forecast models, using the latter to reduce the error of the first.

A second observation arising from this work is the necessity to identify a suitable approach for selecting a DLR value in real-world operation, which has to be selected from the

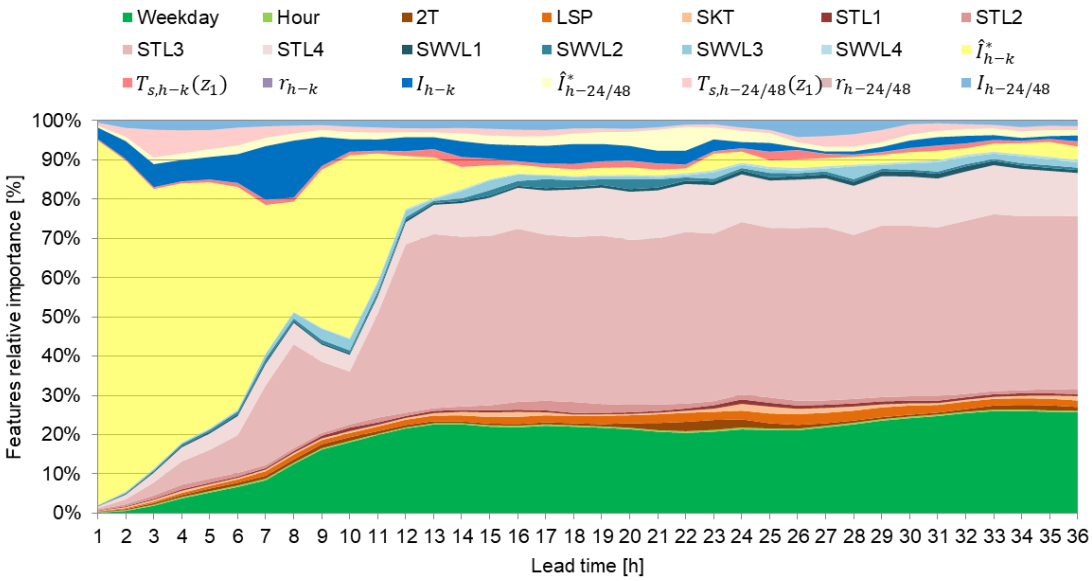


**FIGURE 7.** Relative feature importance from the DDM-RFR clay-soil DLR forecast, for lead times ranging from 1 to 36 hours.

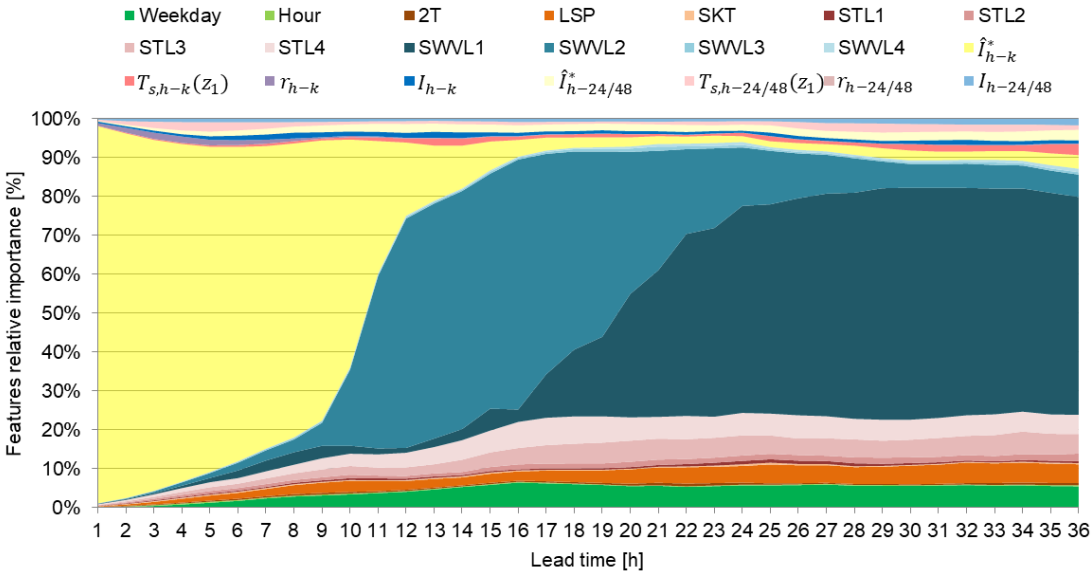


**FIGURE 8.** Relative feature importance from the DDM-RFR sandy-soil DLR forecast, for lead times ranging from 1 to 36 hours.

forecasts by network operators. A first approach could be to use the point forecast provided by the forecasting system and to apply a safety margin to it. This approach has two drawbacks: firstly it does not solve the question on how to define the safety margin, and secondly, it does not solve the problem on how to deal with a variable rating along several horizons. A simple method for defining the safety margin is given by the use of the RMSE, known for each forecast horizon. Assuming the errors to follow a Gaussian distribution, it is possible to define a value on this distribution corresponding to an accepted value of risk. For example, we plot in Figure 9 the forecast value and the resulting value once a safety margin equal to three times the standard deviation is applied, for the sandy-soil case and for all the time horizons. If the operational DLR is set at this value, there would be roughly a probability of 1.5% to have an observation smaller than the operational DLR. Unfortunately, such approach would reduce most of the advantages provided by the use of DLR: for example, the rated current is 142 A and the average DLR is 209 A, (i.e., about 47% greater). Considering that the average DDM-LR RMSE is about 9 A, setting a reduction equal to three times the average RMSE

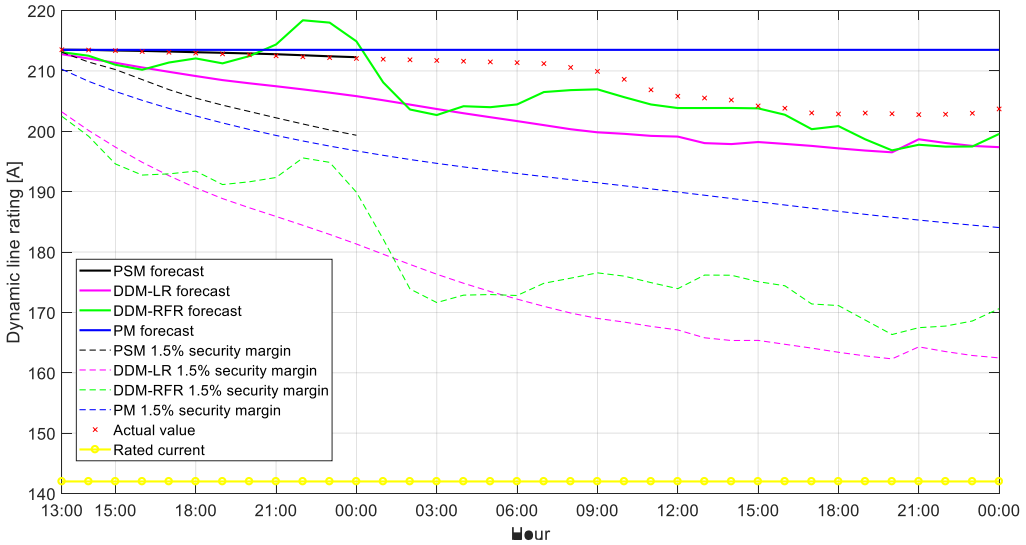


**FIGURE 9.** **Comparison of DLR forecast methods for a UGC buried in sandy soil, for a sample day. The dashed line correspond to 3$\sigma$ intervals, representing a rough 1.5% probability of exceedance.**

for all the horizons, the average applied DLR is 182 A, i.e., only the 28% greater than the rated current. Probabilistic approaches could be suitable to tackle this problem, and they will be the subject of future research.

## VI. CONCLUSIONS

This paper describes a work on the problem of UGC DLR forecasting. Intraday (up to 12 hours ahead) and day-ahead (13 to 36 hours ahead) scenarios are separately investigated, due to the different challenges that arise in these different contexts.

Two methods that make use of the IEC cable-soil dynamic thermal model are investigated in this paper.

A PSM is specifically developed for intraday UGC DLR forecasting. Thermal and hydraulic phenomena occur in the cable-soil system, thus influencing the UGC DLR; for example, cables buried in soils at greater temperature dissipate less heat caused by Joule losses, whereas cables buried in soils at smaller temperature dissipate more heat; this results in an increase (decrease) of the cable temperature. Implementing physical equations that capture the detailed dynamics of thermal and hydraulic phenomena in the forecasting method allows increasing the overall accuracy; however, this tool is computationally intensive, and thus its applicability is limited for short scenarios (intraday forecast).

A DDM, adapted from relevant literature on OHL DLR forecasting, is instead developed and tested for both intraday and day-ahead scenarios. There are two main reasons behind this choice for longer scenarios: the computational complexity of the physical-statistical approach and the forecasting error propagation. The forecasting method must return its output after a reasonable period after its launch; solving thermal and hydraulic dynamic models require more and more time for longer forecasting scenarios until reaching unaffordable computational burden. Moreover, solving thermal and hydraulic dynamic models throughout a longer time interval suffers the propagation of forecasting errors (i.e., the unavoidable errors committed when forecasting variables modify the thermal and hydraulic dynamics until reaching too-large errors for longer scenarios). To cope with this issue, we test a DDM that, starting from historical UGC DLR data, directly aims at forecasting UGC DLR by means of a statistical regression model (i.e., LR or RFR), trained upon actual UGC DLR data. The DDMs make use of NWPs of relevant weather parameters.

The comparison at intraday scenarios demonstrates the superiority of the PSM, compared to the DDMs and to a persistence benchmark. The main reason behind this consists of the differences in the dynamic inertia of the cable-soil system, with respect to the OHL case. This translates in a different distribution of the feature importance in the data-driven approach, which therefore has to be significantly improved before being applicable to the UGC DLR case.

In summary, the study described in this paper, with its comparison of different approaches for a large interval of forecast horizons, presents interesting contributions on the topic of UGC DLR forecast.

Firstly, it allows clarifying the expected performance of UGC DLR forecast algorithms at different horizons.

Secondly, the study clarified the importance of using a dynamic model of the cable-soil system in order to exploit the known information about the large inertia of this system. Information about forecast soil temperature and water content begin to be important only for lead times greater than 12 hours.

Eventually, this paper invites to focus on the best way to draw an operational DLR value from DLR forecasts, providing a simple suggestion based on a risk-based method;

however, its performance in terms of unlocked latent ampacity must be improved.

The work opens new perspectives on this topic such as: i) the best way to integrate a physical and statistical model for UGC DLR forecast, ii) the calculation of probabilistic forecasts, and the definition of a suitable method for using the forecast to select a reliable operational DLR value in intraday and day-ahead scenarios; iii) the inclusion in the forecasting methodology of the moisture migration effect caused by the heating of the zones in close proximity to the cable, by means of finite-element methods and/or simplified procedures; iv) the findings of this study on UGCs in distribution systems (in which the availability of controllable loads or controllable generators is a pre-requisite in order to effectively exploit the latent ampacity of UGC) will be extended, with the necessary amendments, to higher voltage underground transmission lines, in which the re-dispatch of power flows is always desirable.

## ACKNOWLEDGMENT

The authors wish to thank prof. Guido Carpinelli for his support in the development of the methodologies, the European Centre for Medium-range Weather Forecasts (ECMWF) for providing the historical weather forecasts, and the Centre for Environmental Data Analysis (CEDA) for providing the historical weather measurements used in this study.

## REFERENCES

[1] M. Z. Degefa, M. Koivisto, R. J. Millar, and M. Lehtonen, "Dynamic thermal state forecasting of distribution network components: For enhanced active distribution network capacity," in *Proc. Int. Conf. Probab. Methods Appl. Power Syst. (PMAPS)*, Durham, U.K., Jul. 2014, pp. 1–6.

[2] A. Safdarian, M. Z. Degefa, M. Fotuhi-Firuzabad, and M. Lehtonen, "Benefits of real-time monitoring to distribution systems: Dynamic thermal rating," *IEEE Trans. Smart Grid*, vol. 6, no. 4, pp. 2023–2031, Jul. 2015.

[3] A. Michiorri *et al.*, "Forecasting for dynamic line rating," *Renew. Sustain. Energy Rev.*, vol. 52, pp. 1713–1730, Dec. 2015.

[4] *Low-Voltage Electrical Installations—Part 5-52: Selection and Erection of Electrical Equipment—Wiring Systems*, IEC Standard 60364-5-52:2009.

[5] C. J. Wallnerström, Y. Huang, and L. Söder, "Impact from dynamic line rating on wind power integration," *IEEE Trans. Smart Grid*, vol. 6, no. 1, pp. 343–350, Jan. 2015.

[6] E. Fernandez, I. Albizu, M. T. Bedialauneta, A. J. Mazon, and P. T. Leite, "Review of dynamic line rating systems for wind power integration," *Renew. Sustain. Energy Rev.*, vol. 53, pp. 80–92, Jan. 2016.

[7] S. Negari, K. Raahemifar, and D. Xu, "Predictive line rating in underground transmission lines going beyond dynamic line rating," in *Proc. IEEE Can. Conf. Elect. Comput. Eng. (CCECE)*, Vancouver, BC, USA, May 2016, pp. 1–6.

[8] D. Clements, P. Mancarella, and R. Ash, "Application of time-limited ratings to underground cables to enable life extension of network assets," in *Proc. Int. Conf. Probab. Methods Appl. Power Syst. (PMAPS)*, Beijing, China, 2016, pp. 1–7.

[9] Y. Bicen, "Trend adjusted lifetime monitoring of underground power cable," *Electr. Power Syst. Res.*, vol. 143, pp. 189–196, Feb. 2017.

[10] M. Dabbaghjamanesh, A. Kavousi-Fard, and S. Mehraeen, "Effective scheduling of reconfigurable microgrids with dynamic thermal line rating," *IEEE Trans. Ind. Electron.*, vol. 66, no. 2, pp. 1552–1564, Feb. 2019.

[11] L. Jenkins, N. Fahmi, and J. Yang, "Application of dynamic asset rating on the UK LV and 11 kV underground power distribution network," in *Proc. 52nd Int. Univ. Power Eng. Conf. (UPEC)*, Heraklion, Greece, 2017, pp. 1–6.

[12] R. Huang, J. A. Pilgrim, P. L. Lewin, D. Scott, and D. Morrice, "Use of day-ahead load forecasting for predicted cable rating," in *Proc. IEEE PES Innov. Smart Grid Technol., Eur. (ISGT Europe)*, Istanbul, Turkey, Oct. 2014, pp. 1–6.

[13] R. Huang, J. A. Pilgrim, P. L. Lewin, and D. Payne, "Dynamic cable ratings for smarter grids," in *Proc. IEEE PES Innov. Smart Grid Technol. Eur. (ISGT Europe)*, Lyngby, Denmark, Oct. 2013, pp. 1–5.

[14] H. J. Li, K. C. Tan, and Q. Su, "Assessment of underground cable ratings based on distributed temperature sensing," *IEEE Trans. Power Del.*, vol. 21, no. 4, pp. 1763–1769, Oct. 2006.

[15] Y. C. Liang and Y. M. Li, "On-line dynamic cable rating for underground cables based on DTS and FEM," *WSEAS Trans. Circuits Syst.*, vol. 7, no. 4, pp. 229–238, 2008.

[16] A. Michiorri, P. C. Taylor, S. C. E. Jupe, and C. J. Berry, "Investigation into the influence of environmental conditions on power system ratings," *Proc. Inst. Mech. Eng., A, J. Power Energy*, vol. 223, no. 7, pp. 743–757, 2009.

[17] R. Olsen, G. J. Anders, J. Holboell, and U. S. Gudmundsdottir, "Modelling of dynamic transmission cable temperature considering soil-specific heat, thermal resistivity, and precipitation," *IEEE Trans. Power Del.*, vol. 28, no. 3, pp. 1909–1917, Jul. 2013.

[18] R. S. Olsen, J. Holboll, and U. S. Gudmundsdóttir, "Dynamic temperature estimation and real time emergency rating of transmission cables," in *Proc. IEEE Power Energy Soc. Gen. Meeting*, San Diego, CA, USA, Jul. 2012, pp. 1–8.

[19] J. L. Aznarte and N. Siebert, "Dynamic line rating using numerical weather predictions and machine learning: A case study," *IEEE Trans. Power Del.*, vol. 32, no. 1, pp. 335–343, Feb. 2017.

[20] R. Dupin, A. Michiorri, and G. Kariniotakis, "Dynamic line rating day-ahead forecasts—Cost benefit based selection of the optimal quantile," in *Proc. CIRED Workshop*, Helsinki, Finland, 2016, pp. 1–4.

[21] *Electric Cables—Calculation of the Current Rating—Part 2-1: Thermal Resistance—Calculation of the Thermal Resistance*, IEC Standard 60287-2-1:2015.

[22] G. J. Anders, *Rating of Electric Power Cables: Ampacity Computations for Transmission, Distribution, and Industrial Applications*. New York, NY, USA: McGraw-Hill, 1997.

[23] A. Morello, "Variazioni transitorie di temperatura nei cavi per energia," *L'Elettrotecnica*, vol. 45, no. 4, pp. 213–222, 1958.

[24] N. H. Abu-Hamdeh, "Thermal properties of soils as affected by density and water content," *Biosyst. Eng.*, vol. 86, no. 1, pp. 97–102, 2003.

[25] N. Diao, Q. Li, and Z. Fang, "Heat transfer in ground heat exchangers with groundwater advection," *Int. J. Therm. Sci.*, vol. 43, no. 12, pp. 1203–1211, 2004.

[26] M. A. Celia, E. T. Bouloutas, and R. L. Zarba, "A general mass-conservative numerical solution for the unsaturated flow equation," *Water Resour. Res.*, vol. 26, no. 7, pp. 1483–1496, 1990.

[27] M. T. van Genuchten, "A closed-form equation for predicting the hydraulic conductivity of unsaturated soils," *Soil Sci. Soc. Amer. J.*, vol. 44, no. 5, pp. 892–898, 1980.

[28] S. Manfreda, T. M. Scanlon, and K. K. Caylor, "On the importance of accurate depiction of infiltration processes on modelled soil moisture and vegetation water stress," *Ecohydrology*, vol. 3, no. 2, pp. 155–165, 2010.

[29] I. Rodríguez-Iturbe, V. Isham, D. R. Cox, S. Manfreda, and A. Porporato, "Space-time modeling of soil moisture: Stochastic rainfall forcing with heterogeneous vegetation," *Water Resour. Res.*, vol. 42, no. 6, pp. 1–11, 2006.

[30] A. J. Smola and B. Schölkopf, "A tutorial on support vector regression," *Statist. Comput.*, vol. 14, no. 3, pp. 199–222, Aug. 2004.

[31] L. Breiman, "Random forests," *Mach. Learn.*, vol. 45, no. 1, pp. 5–32, 2001.

[32] F. J. Leij, W. J. Alves, M. T. van Genuchten, and J. R. Williams, "Unsaturated soil hydraulic database, UNSODA 1.0 user's manual," U.S. Environ. Protection Agency, Washington, DC, USA, Tech. Rep. EPA/600/R96/095, 1996.

[33] *Met Office Integrated Data Archive System (MIDAS) Land and Marine Surface Stations Data (1853-Current)*, NCAS Brit. Atmos. Data Centre, Leeds, U.K., 2012.

[34] *European Centre for Medium Range Weather Forecasts (ECMWF)*. Accessed: Feb. 2018. [Online]. Available: https://www.ecmwf.int/fr

**ANTONIO BRACALE** (M'04–SM'17) received the degree in telecommunication engineering from the University of Napoli Federico II, Italy, in 2002, and the Ph.D. degree in electrical energy conversion from the Second University of Napoli, Italy, in 2005.

He is currently an Associate Professor in electrical power systems with the Department of Engineering, University of Napoli Parthenope, Italy. His research interests mainly include power quality, power systems analysis, and energy forecasting.

**PIERLUIGI CARAMIA** received the M.Sc. degree in electrical engineering from the University of Cassino, Italy, in 1991.

He is currently an Associate Professor in electrical power systems with the Department of Engineering, University of Napoli Parthenope, Italy. His research interests mainly include power quality, cable rating, and power system analysis.

**PASQUALE DE FALCO** (M'18) received the B.S. and M.Sc. degrees in electrical engineering and the Ph.D. degree in information technology and electrical engineering from the University of Napoli Federico II, Italy, in 2011, 2014, and 2018, respectively.

He is currently a Postdoctoral Researcher with the Department of Engineering, University of Napoli Parthenope, Italy. His research interests mainly include energy forecasting and energy data analytics.

**ANDREA MICHIORRI** received the M.Sc. degree in mechanical engineering with a specialization in energy from the University of Rome La Sapienza, Italy, in 2005, and the Ph.D. degree from the University of Durham, in 2010, with a dissertation on the thermal state estimation of power system components.

He is currently a Researcher with the Centre procédés, énergies renouvelables et systèmes énergétiques, MINES ParisTech, Sophia Antipolis, France. His research interests mainly include the integration of renewable sources and distributed generators into power systems, with a particular focus on the aspects of decision-making under uncertainty.

**ANGELA RUSSO** (M'16–SM'18) received the M.Sc. degree in electrical engineering and the Ph.D. degree in industrial engineering from the University of Cassino, Italy, in 1996 and 2000, respectively.

She is currently an Associate Professor in electrical power systems with the Department of Energy, Politecnico of Torino, Italy. Her research interests mainly include power quality, power system analysis, and energy forecasting.